Available online at www.sciencedirect.com

SciVerse ScienceDirect

Geochimica et Cosmochimica Acta 75 (2011) 7688–7697

Geochimica et Cosmochimica Acta

www.elsevier.com/locate/gca

High-temperature Si isotope fractionation between iron metal and silicate

Anat Shahar [a,*], Valerie J. Hillgren [a], Edward D. Young [b], Yingwei Fei [a], Catherine A. Macris [b], Liwei Deng [a]

[a] Geophysical Laboratory, Carnegie Institution of Washington, 5251 Broad Branch Rd. NW, Washington, DC 20015, United States
[b] Department of Earth and Space Sciences, UCLA, 595 Charles Young Drive East, 2676 Geology, Los Angeles, CA 90095, United States

Received 19 April 2011; accepted in revised form 26 September 2011; available online 2 October 2011

Abstract

The Si stable isotope fractionation between metal and silicate has been investigated experimentally at 1800, 2000, and 2200 °C. We find that there is a significant silicon stable isotope fractionation at high temperature between metal and silicate in agreement with Shahar et al. (2009). Further we find that this fractionation is insensitive to the structure and composition of the silicate as the fractionation between silicate melt and olivine is insignificant within the error of the analyses. The temperature-dependent silicon isotope fractionation is $\Delta^{30}Si_{silicate-metal} = 7.45 \pm 0.41 \times 10^6/T^2$. We also demonstrate the viability of using laser ablation MC-ICPMS as a tool for measuring silicon isotope ratios in high pressure and temperature experiments.

1. INTRODUCTION

The composition of the interior of our planet has been studied extensively with a variety of approaches. Experiments, calculations, and laboratory measurements have all been used to shed light on the element(s) responsible for the observed density deficit in Earth's core. The recent (debated) discovery that the silicate Earth's silicon isotope ratios are different than the silicon isotope ratios in primitive meteorites (Georg et al., 2007; Fitoussi et al., 2009; Chakrabarti and Jacobsen, 2010) has prompted a series of studies aimed at assessing the utility of using stable isotope ratios as tracers of the composition of the core. There is little agreement on the exact difference between the $^{30}Si/^{28}Si$ ratios of the silicate Earth and chondrite (Georg et al., 2007; Fitoussi et al., 2009; Chakrabarti and Jacobsen, 2010; Savage et al., 2010; Ziegler et al., 2010; Armytage et al., 2011). However, while the exact value is not agreed upon, most studies show that there is indeed a discernible difference between bulk silicate Earth and primitive meteorites. The one exception is the study by Chakrabarti and Jacobsen (2010) in which the authors find no difference in the silicon isotopic ratios of meteorites and Earth. It is unclear why their data differ. Nonetheless, if the silicon isotope ratios of bulk silicate Earth (BSE) differ from the silicon isotope ratios of the supposed building blocks of the Earth (chondrites), then some process must have occurred during Earth formation to create the difference. One obvious way to segregate Si isotopes is through silicon incorporation into the metallic iron diapirs that sank and formed the Earth's core (e.g., Wade and Wood, 2005). The notion that the core contains Si is not new. It has been known for quite some time that the Mg/Si and Al/Si ratios in the bulk silicate Earth are superchondritic, that is, that there is a deficit of Si in the bulk silicate Earth relative to Mg and Al (e.g., Palme and O'Neil, 2003). Because Si easily alloys with Fe under reducing conditions (see Hillgren et al., 2000 or Li and Fei, 2004 for a review), Si is considered to be among the most plausible candidates for the Earth's outer core density deficit. Silicon sequestration in

* Corresponding author. Tel.: +1 202 478 8929.
E-mail address: ashahar@ciw.edu (A. Shahar).

0016-7037/$ - see front matter © 2011 Elsevier Ltd. All rights reserved.
doi:10.1016/j.gca.2011.09.038

the core relies on core–mantle equilibration at conditions more reducing than the current oxidation state of the Earth's mantle. The combination of the isotope fractionation factor between silicate and Fe–Si alloy and the difference in $^{30}Si/^{28}Si$ between BSE and chondrites could be used to estimate the amount of Si incorporated into the core at a given formation temperature.

This study combines experiments at high pressure and temperature with isotope analyses by laser ablation multiple collector inductively coupled plasma mass spectrometer (LA-MC-ICPMS) in order to better constrain the silicon isotope fractionation factor between silicate and Fe-rich metal at conditions relevant to Earth's interior. We extend the single previous experimental study to several temperatures so as to determine experimentally the temperature dependence of the Si isotope fractionation factor, and introduce laser ablation MC-ICPMS as an important technique for measuring isotope fractionation in experiments. We also discuss the requirements for demonstrating isotopic equilibrium in experimental charges and examine the influence of choice of experimental capsule material on isotope fractionation factor determinations.

2. METHODOLOGY

2.1. High pressure experiments

Experiments were conducted on the Geophysical Laboratory's piston cylinder and multi-anvil presses at 1 and 7 GPa, respectively. The 1 GPa cell assembly consists of a graphite tube heater insulated by a Pyrex glass sleeve and talc shell. A W/Re thermocouple is inserted into the sample chamber through a small hole in the stainless steel base plug, which is surrounded by a small pyropholite sleeve. The 7 GPa cell assembly consists of an 18 mm edge length cast MgO ceramic octahedra with a zirconia-insulating sleeve surrounding a graphite heater (Bertka and Fei, 1997). A W/Re thermocouple is in contact with the top of the sample capsule. Experiments were performed at 1800, 2000 and 2200 °C for durations ranging from 15 to 60 min. MgO or graphite capsules were used in all experiments. Table 1 lists all the experiments and conditions. Experiments at 7 GPa were annealed at 1400 °C for 2–4 h prior to increasing to the temperature of interest in order to strengthen the capsule material. The starting composition was identical to that used previously (Shahar et al., 2009) and consisted of a silicate–oxide mix of Al_2O_3, MgO, SiO_2, CaO and Fe_2O_3 in proportions representing a pyrolitic BSE composition and a metallic iron-silicon alloy (Fe with 9 wt.% Si) powder in a 1:2 ratio. The silicate starting material was spiked with ^{28}Si in order to trace the exchange of Si between the phases as discussed below and in detail in Shahar et al. (2009).

2.2. Characterization of experimental run products

Samples were recovered and polished. They were examined with the SEM, and the elemental composition was determined with the 5-spectrometer JEOL 8900 electron probe microanalyzer (EPMA) at the Geophysical Laboratory. The 7 GPa samples consisted of liquid Fe–Si metallic alloy, dendritic liquid silicate, olivine, and MgO capsule material. The liquid silicate was located on the edge of the sample in all cases and was mixed thoroughly with the MgO capsule. The quenched Fe–Si alloy in these samples showed some dendritic texture with small blobs (Fig. 1). The 1 GPa samples contained liquid Fe–Si alloy, olivine, and a pyroxene, but no silicate liquid. We used diopside, sillimanite, and hematite for Si standards in the silicate, Mg, Ca, Al, and O, pure metal standards for Si in the metal, Fe, Mn, Re, and W, and graphite for C. We analyzed for Re and W to check for contamination from the thermocouple. We used an accelerating voltage of 15 keV, a beam current of 30 nA, and peak counting times ranging from 30 to 60 s. Analyses were reduced using a ZAF correction routine.

A point beam was used to measure the olivines, pyroxenes and the metal in run PC871. The dendritic liquid silicate was analyzed by rastering the beam over an approximately 15 μm area. On the order of twenty analyses were made and averaged together to arrive at the composition of the liquid. To measure the Fe–Si alloys for the 7 GPa samples we also rastered over an approximately 15 μm area then averaged 40–70 analyses to give an integrated analysis of the alloy plus the blobs which are interpreted to be a quench product (e.g., see Geßmann and Rubie, 1998; O'Neill et al., 1998). A comparison of the metal composition with and without the blobs shows a difference in the Si content of only 0.2 wt.%. Therefore, their inclusion or exclusion from the LA-MC-ICPMS analysis should have little or no effect on the ratio of the Si isotopes. The metal totals for runs PL613 and PR892 were consistently low suggesting that the metal had become contaminated with C during the run (presumably from the heater, but contamination of the starting material during loading cannot be ruled out). To determine the C content of the metal, we analyzed for C without removing the C coat and then re-reduced the data using a correction for a thin film of C. PL613, PR892, PR855, and PC871 were all carbon coated together and therefore the carbon coat should have

Table 1
Experimental conditions.

Experiment	Pressure (Gpa)	Temperature (°C)	Time (min)	Capsule material
PL613	7	2200	20	MgO
PR892	7	2000	30	MgO
PC871	1	1800	60	MgO
PC868	1	1800	60	C
PR846	7	2000	15	C

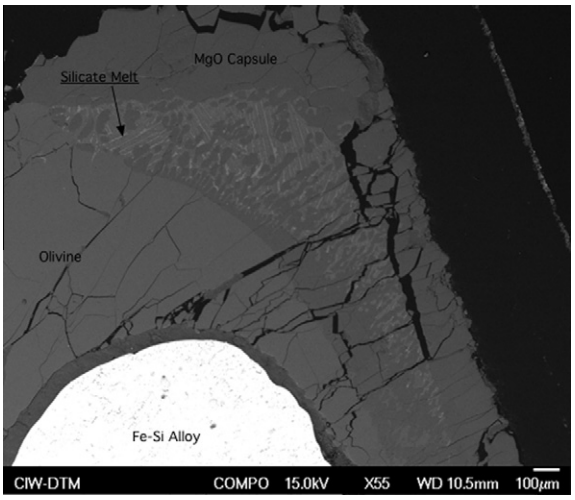

Fig. 1. A photograph of PR892 showing the olivine, silicate melt, MgO capsule and Fe–Si alloy. The rim surrounding the Fe–Si alloy is alumina polishing compound filling in a crack in the sample.

the same thickness on all the samples. PC871 was assumed to have no C in the metal since its totals were reasonable when analyzed without including C, so it was used as a standard to calculate the carbon coat thickness. The other samples were then assumed to have that C coat thickness and the thin film correction was made to determine how much of the analyzed C was in the sample vs. the C-coat. Average EPMA analyses of the experimental run products from samples run in MgO capsules are shown in Table 2. Samples run in graphite capsules are briefly discussed in the results section.

2.3. Isotope ratio analysis: laser ablation MC-ICPMS

Following the work of Shahar and Young (2007) and Ziegler et al. (2010) we used the Thermo Scientific Neptune MC-ICPMS at UCLA to analyze the silicon isotopic ratios of the experimental run products. Three Faraday collectors were spaced to collect $^{28}Si^{+}$, $^{29}Si^{+}$, and $^{30}Si^{+}$ simultaneously. Potential molecular interferences ($^{12}C^{16}O^{+}$, $^{28}N_2^{+}$, $^{28}SiH^{+}$, $^{14}N^{16}O^{+}$) were resolved by operating at a mass resolving power of ~8000. Corrections for instrumental mass bias were performed by sample-standard bracketing using San Carlos olivine as our in-house standard. Isotope analyses were corrected by subtracting a preceding on-peak background measurement. Typical $^{29}Si^{+}$ signal intensities during measurements were ~230 mV and backgrounds for $m/z = 28$, 29, and 30 were 92, 4, and 3 mV, respectively. Isotope ratio measurements during laser ablation consist of the mean of ten ~4 s integration cycles.

We used a 193 nm excimer laser (Photon Machines, Analyte 193) operated with a pulse repetition rate of 2 (silicate) to 5 (metal) Hz and UV fluence of ~22 J/cm^2. Cylindrical ablation pit diameters varied between 86 - microns in the silicate and 172 microns in the metal and were approximately 30–50 microns deep. Ablation products were flushed from the ablation cell in a flow of He gas (0.52 L/min) and then mixed with Ar (0.64 L/min) and N_2

Table 2
Electron probe microanlayzer analyses of the experimental run products.

	Fe	Al	Ca	Si	Re	Mg	Mn	W	O[a]	C	Total
PR892											
Olivine	0.19 (0.02)	0.17 (0.05)	0.18 (0.03)	19.91 (0.45)	0.03 (0.03)	33.87 (0.36)	0.04 (0.007)	NA	45.37 (0.78)	NA	99.77
Liquid silicate	0.32 (0.02)	2.17 (0.40)	4.25 (0.71)	19.13 (0.70)[b]	0.06 (0.01)	28.76 (0.91)	0.07 (0.01)	NA	44.52 (0.64)[b]	NA	99.27
Metal	90.92 (0.58)	0.29 (0.006)	BD	7.01 (0.07)	0.03 (0.03)	0.01 (0.005)	0.10 (0.02)	0.02 (0.03)	0.49 (0.08)	2.53 (0.84)	101.40
PL613											
Olivine	0.14 (0.07)	0.19 (0.06)	0.27 (0.06)	19.83 (0.40)	0.01 (0.02)	33.70 (0.36)	0.03 (0.02)	NA	45.15 (0.69)	NA	99.46
Liquid silicate	0.19 (0.03)	1.70 (0.24)	3.80 (0.51)	19.82 (0.25)[b]	0.05 (0.01)	29.71 (0.75)	0.05 (0.003)	NA	45.37 (0.51)[b]	NA	100.97
Metal	90.49 (0.49)	0.04 (0.013)[c]	BD	7.18 (0.06)	0.03 (0.04)	BD	0.11 (0.02)	0.03 (0.03)	0.37 (0.05)	1.42 (0.98)	99.67
PC 871											
Olivine	0.12 (0.05)	0.11 (0.12)	0.21 (0.12)	19.56 (0.10)	BD	34.12 (0.30)	0.04 (0.01)	0.01 (0.01)	45.02 (0.27)	NA	99.20
Pyroxene	0.13 (0.02)	11.18 (0.39)	16.47 (0.14)	20.23 (0.03)	0.02 (0.02)	7.04 (0.29)	0.15 (0.002)	BD	33.34 (0.22)	NA	99.57
Metal	93.04 (0.49)	BD	BD	8.11 (0.03)	0.03 (0.04)	BD	0.12 (0.01)	0.01 (0.03)	0.32 (0.02)	0.00[d]	101.63

Except for where otherwise noted, for the solid silicates and metals, the numbers in parenthesis are the standard deviations among the analyses, and for the liquid silicates it is the standard deviation of the means. BD – below detection, NA – not analyzed for.

[a] Oxygen content of silicates was calculated based on valencies assumed for the cations. Oxygen in the metal was directly measured.

[b] Because there was little variance between analyses, the standard deviation of the means gives an unreasonably low error so the standard deviation of the analyses was used.

[c] Standard deviation of the means was used because element content varied greatly due the presence of blobs.

[d] C was defined as 0 in this sample to act as a standard to determine carbon coat thickness.

gas (6–10 mL/min) before introduction to the mass spectrometer. The addition of the nitrogen gas was essential to increasing the sensitivity of the instrument however, it also served to increase the background (especially $m/z = 28$). As the intensity of the three beams was large relative to the background and the background was stable, resulting from a steady flow of N_2, on-peak subtraction of background was used for all measurements.

We tested the accuracy of our results by ablating a synthetic glass ($Di_{0.59}An_{0.41}$) prepared with 1% ^{28}Si spike as discussed in Shahar and Young (2007). Accuracy of isotope ratios was found to be dependent on the distance of the torch from the sample cone of the mass spectrometer. This is a phenomenon that is widely understood as being due to changing the position within the plasma at which the sample is introduced (Pearson et al., 2008). As the torch moves away from the cones the plasma being sampled decreases in temperature. This effect changes the mass bias. While this is not much of a problem for solutions, laser ablation is especially sensitive to torch position. For example, in laser ablation runs standard and sample do not have the same matrix composition and therefore standard sample bracketing does not compensate for the torch being in a less than optimal position. Accordingly, in order to ensure accuracy the torch position was fine tuned several times each day using materials of known isotopic composition. In practice the optimal torch position was found to be stable a day to several days. Precision of the LA-MC-ICPMS analyses is on the order of $\pm 0.4‰$ 2σ for $\delta^{30}Si$. As NBS-28 (an international Si standard) is a powdery substance that cannot be analyzed easily by an excimer laser, we calibrated our analyses by measuring a sample of San Carlos olivine relative to NBS-28 by solution and using this San Carlos olivine as our in-house laser ablation standard. The $\delta^{29}Si$ of our in-house San Carlos standard relative to NBS-28 is -0.21 ± 0.06 (2se)‰ (Ziegler et al., 2010). Fig. 2 shows approximately 250 measurements of the in-house standard plotted relative to NBS-28 showing the long-term reproducibility and accuracy.

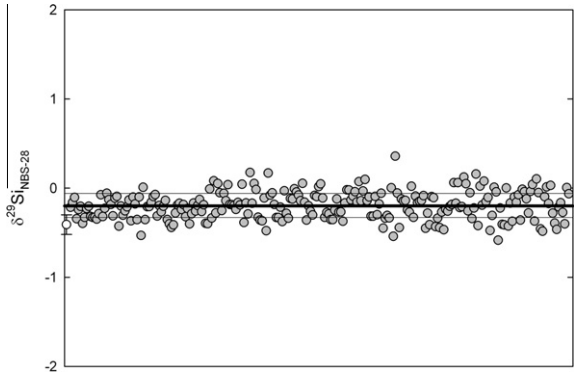

Fig. 2. Approximately 250 laser ablation MC-ICPMS standard (San Carlos olivine shown relative to NBS-28) analyses. Bold line indicates the true value of SC Olivine relative to NBS-28 (−0.20‰) and two thinner lines indicate typical 2σ error. Scatter is mostly due to instrumental drift. The white data point is from Chmeleff et al. (2008) and is obtained by femtosecond laser ablation MC-ICPMS.

The accuracy of our laser ablation methods is within 0.1–0.2 per mil ($\delta^{30}Si$) of results obtained by solution, including those for Fe-rich Si-bearing metal (Ziegler et al., 2010). In the latter study Ziegler et al. (2010) ablated a metal rich portion of an enstatite chondrite and showed that it was within error of the solution analyses of the same material. Matrix effects (with the exception of carbon, detailed below) were not seen within run products, even when using San Carlos olivine as a standard for the Fe–Si alloy. We also verified the accuracy of silicate analyses using the conditions used for metal analyses (5 Hz, 172 μm diameter) to ensure against a bias imposed by spot size or pulse rate. Fig. 3 shows typical laser ablation pits in an experimental charge consisting of olivine, silicate melt, and Fe-rich Si-bearing metal.

Most of the experiments were analyzed on two separate days spaced in time by of order one month. This procedure reduces the risk of biases to data from any given session of analyses, as discussed below. All analyses are reported in traditional δ notation:

$$\delta^{29(30)}\mathrm{Si} = \left(\frac{R_{\mathrm{sample}}}{R_{\mathrm{standard}}} - 1\right) * 1000,$$

where $R = {}^{29}Si/{}^{28}Si$ or $^{30}Si/{}^{28}Si$. Fractionation factors between metal and silicate are reported as $\Delta^{30}Si_{\text{silicate-metal}} = \delta^{30}Si_{\text{silicate}} - \delta^{30}Si_{\text{metal}}$.

2.4. Equilibrium

The three-isotope technique was used in order to help establish attainment of isotopic equilibrium in the experiments (Matsuhisa et al., 1978; Shahar et al., 2008, 2009). Briefly, the starting oxides were spiked with ^{28}Si thereby displacing the bulk isotopic system from the terrestrial

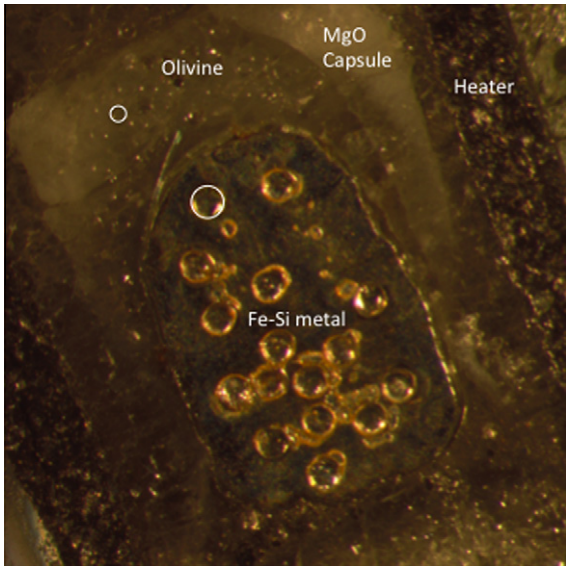

Fig. 3. A picture of PR-892. The heater, MgO capsule, olivine and Fe–Si metal are shown and noted. The two circles show the size of the laser ablation spots, olivine spots are 86 microns and metal spots are 172 microns.

fractionation line on a plot of $\delta^{29}Si$ vs. $\delta^{30}Si$. Once the experimental system is brought up to the pressure (P) and temperature (T) of interest the isotopes mix and align on the experimental mass fractionation line (secondary fractionation line), the position of which on a plot of $\delta^{29}Si$ vs. $\delta^{30}Si$ is defined by the amount of ^{28}Si added to the system. Previous experiments in the Si isotope system (Shahar et al., 2009) were based on the same starting compositions. As a result, the position of the secondary mass fractionation line for these starting compositions is known to high precision based on solution MC-ICPMS measurements. One criterion for isotopic equilibrium in these experiments is that all of the run products must lie on the secondary fractionation line that passes through the bulk composition of the system.

This coincidence of the data for both silicate and metal with the secondary mass fractionation line is not in itself enough to prove isotopic equilibrium in systems where melt is produced such as in the Shahar et al. (2009) study. Molten samples will lie on the same fractionation line simply due to rapid mixing prior to equilibration. In this study the fractionation is between olivine and iron melt and therefore is at equilibrium if the olivine is on the same fractionation line as the metal. In our previous work (Shahar et al., 2009) we showed that isotopic equilibrium between metal and silicate was achieved at 1800 °C after 30 min. We have run one duplicate for 60 min to confirm that result as part of this study. The experiments in this study were run for 20 min (2200 °C) to 60 min (1800 °C).

3. RESULTS

3.1. Isotopic results

Table 3 lists the laser ablation MC-ICPMS analyses obtained on all experimental charges performed in MgO capsules. Fig. 4 shows the three isotope plots for the experiments. All data points plot on the same experimental secondary fractionation line that passes through the bulk composition of the system, satisfying the criteria for isotopic equilibrium and implying that no Si was lost during the experiment; the system was truly closed to mass transfer of Si. In all cases the silicate is more enriched in the heavy isotopes than the coexisting metal. Samples PC871 (Fig. 4a) and PR892 (Fig. 4b) show no obvious correlation with the date of analysis. That is, all analyses on the metal and silicate irrespective of the analysis date show similar values. However, PL613 (Fig. 4c) shows a clear offset between the December 2010 analyses and the January 2011 analyses. While the isotope ratio values differ, the difference between the silicate and metal are the same for both sessions (Fig. 4c). This implies that the absolute shift in measured ratios from one day to the next was a bias due to the laser ablation-mass spectrometry and does not influence the $\Delta^{30}Si_{silicate-metal}$ for the experiment. Results for the $\Delta^{30}Si_{silicate-metal}$ based on olivine–metal pairs are $1.77 \pm 0.32‰$ at 1800 °C, $1.52 \pm 0.23‰$ at 2000 °C, and $1.07 \pm 0.43‰$ at 2200 °C.

No analyses could be made of the isotopic composition of the quenched silicate melt in the 7 GPa experiments as the Si signal was too weak and there was metal contamination in each attempt. In both PR892 and PL613 the silicate melt was seen near one of the edges of the capsule with tiny blebs of metal throughout. There were no areas large enough to ablate without contamination from the metal portion. The majority of the silicon however was in the olivine phase as olivine was the main silicate phase. Two experiments done in graphite capsules (PC868 and PR846) could not be analyzed due to a graphite matrix effect. In general, laser ablation MC-ICPMS analyses of samples from graphite capsules proved untrustworthy as they were inconsistent and irreproducible and therefore were not used in this study. If samples are to be analyzed from experiments done in graphite capsules, they must be analyzed by solution, not laser ablation MC-ICPMS.

4. DISCUSSION

4.1. Description of experimental run products

4.1.1. PC871 and comparison to previous data

The purpose of this experiment was to duplicate the results of Shahar et al. (2009) to confirm that those experiments represented equilibrium, and to test whether the departure from the mass fractionation line in that study, apparently due to Si loss to the graphite capsule material, and the presence of C in the metal, affected the fractionation measurements.

We find that the fractionation in this experiment duplicates the earlier results of Shahar et al. (2009) ($1.87 \pm 0.14‰$ vs. $1.77 \pm 0.31‰$ in the current study). This agreement has several important implications: (1) while the graphite capsule resulted in an open system for Si, it did not change the measured Si isotope fractionation; (2) thirty minutes was a long enough duration to establish equilibrium conditions; and (3) the presence of several weight percent C in the metal did not change the Si isotope fractionation between carbon and metal. In addition, because the silicates in this sample were solid and the silicates in the samples in Shahar et al. (2009) were liquid, this demonstrates that there is no isotope fractionation between solid and liquid silicates. We note that analyzing experiments by laser ablation has distinct advantages compared with analyses by acid digestion and solution in that heterogeneities on the scale of the experimental charge can be characterized and investigated.

The runs from the MgO capsule reported here and replicating the Shahar et al. (2009) conditions all lie on the secondary mass fractionation line defined by the bulk composition of the charge and so we conclude that the departures from the secondary fractionation line in the earlier study were indeed explained by Si loss to the graphite capsule.

In this experiment, the metal $\delta^{30}Si$ values span 1‰ and the silicate values span 1.3 ‰. These values are not within the error associated with the analysis and are therefore evidently real deviations (external precision is on order 0.4‰ in $\delta^{30}Si$ as noted above). This scatter implies that there is a kinetic process inhibiting the homogenization of the isotopes on the micron scale. As this is the case for all the

Table 3
Laser ablation MC-ICPMS analyses of all experimental run products.

Sample	$\delta^{29}Si_{USNM}$[a]	$\delta^{30}Si_{USNM}$[a]	$\Delta^{29}Si$	$\delta^{29}Si_{NBS-28}$	$\delta^{30}Si_{NBS-28}$
PL613_Sil1	−6.28	−6.52	−2.90	−6.48	−6.84
PL613_Sil2	−6.08	−6.32	−2.81	−6.28	−6.64
PL613_Sil3	−6.26	−6.57	−2.86	−6.46	−6.88
PL613_Sil4	−6.34	−6.71	−2.86	−6.54	−7.03
PL613_Sil5	−6.25	−6.70	−2.78	−6.45	−7.01
PL613_Met1	−6.89	−7.46	−3.03	−7.09	−7.77
PL613_Met2	−6.80	−7.66	−2.83	−7.00	−7.97
PL613_Met3	−6.70	−7.42	−2.86	−6.91	−7.73
PL613_Sil7	−6.68	−7.17	−2.96	−6.88	−7.49
PL613_Sil8	−6.61	−7.51	−2.72	−6.81	−7.82
PL613_Sil9	−6.50	−7.27	−2.74	−6.71	−7.58
PL613_Met4	−7.22	−8.54	−2.80	−7.42	−8.85
PL613_Met5	−7.21	−8.19	−2.97	−7.42	−8.50
PL613_Met6	−7.19	−8.25	−2.92	−7.40	−8.57
PL613_Met7	−7.09	−7.93	−2.99	−7.30	−8.24
PC871_Sil1	−6.27	−6.60	−2.85	−6.47	−6.91
PC871_Sil2	−6.63	−7.08	−2.96	−6.84	−7.40
PC871_Sil3	−6.75	−7.23	−3.01	−6.95	−7.54
PC871_Sil4	−6.64	−7.27	−2.87	−6.84	−7.59
PC871_Met1	−7.20	−8.01	−3.05	−7.41	−8.33
PC871_Met2	−7.40	−8.47	−3.01	−7.60	−8.78
PC871_Met3	−7.39	−8.37	−3.06	−7.59	−8.68
PC871_Sil5	−6.49	−7.09	−2.82	−6.70	−7.40
PC871_Sil6	−6.73	−7.21	−3.00	−6.94	−7.53
PC871_Sil7	−6.79	−7.42	−2.95	−7.00	−7.73
PC871_Sil8	−6.14	−6.64	−2.70	−6.35	−6.96
PC871_Sil9	−6.35	−6.66	−2.91	−6.56	−6.97
PC871_Sil10	−6.08	−6.11	−2.91	−6.28	−6.42
PC871_Sil11	−6.31	−6.58	−2.91	−6.52	−6.90
PC871_Sil12	−6.31	−6.75	−2.82	−6.51	−7.06
PC871_Sil13	−6.21	−6.32	−2.94	−6.41	−6.63
PC871_Sil14	−6.71	−6.69	−3.24	−6.91	−7.00
PC871_Sil15	−6.48	−6.77	−2.98	−6.69	−7.08
PC_871_Met4	−7.60	−8.84	−3.02	−7.81	−9.16
PC_871_Met5	−7.51	−8.78	−2.96	−7.71	−9.09
PC_871_Met6	−7.48	−8.73	−2.96	−7.68	−9.04
PC_871_Met7	−7.66	−8.97	−3.02	−7.87	−9.29
PR892_Sil1	−6.42	−6.87	−2.86	−6.62	−7.19
PR892_Sil2	−6.51	−7.08	−2.85	−6.72	−7.39
PR892_Sil3	−6.50	−6.74	−3.01	−6.70	−7.05
PR892_Sil4	−6.34	−6.22	−3.12	−6.54	−6.53
PR892_Sil5	−6.76	−6.92	−3.18	−6.97	−7.24
PR892_Sil6	−6.81	−7.31	−3.02	−7.01	−7.62
PR892_Sil7	−6.35	−6.82	−2.82	−6.55	−7.13
PR892_Met1	−7.18	−8.08	−3.00	−7.38	−8.39
PR892_Met2	−7.21	−8.16	−2.98	−7.41	−8.48
PR892_Met3	−7.12	−7.92	−3.02	−7.33	−8.23
PR892_Met4	−7.11	−7.84	−3.05	−7.31	−8.15
PR892_Met5	−7.12	−8.16	−2.89	−7.32	−8.47
PR892_Sil12	−6.45	−6.86	−2.89	−6.65	−7.18
PR892_Sil13	−6.62	−6.94	−3.03	−6.82	−7.25
PR892_Sil14	−6.28	−6.32	−3.01	−6.48	−6.63
PR892_Sil15	−6.05	−5.92	−2.99	−6.25	−6.23
PR892_Sil16	−6.21	−6.19	−3.01	−6.42	−6.50
PR892_Sil17	−6.47	−6.88	−2.91	−6.67	−7.19
PR892_Sil18	−6.32	−6.44	−2.99	−6.52	−6.75
PR892_Sil19	−6.53	−6.75	−3.04	−6.74	−7.06
PR892_Sil20	−6.50	−6.92	−2.92	−6.71	−7.24
PR892_Sil21	−6.23	−6.12	−3.07	−6.44	−6.43
PR892_Sil22	−6.60	−7.17	−2.89	−6.81	−7.49

Table 3 (*continued*)

Sample	$\delta^{29}Si_{USNM}$[a]	$\delta^{30}Si_{USNM}$[a]	$\Delta^{29}Si$	$\delta^{29}Si_{NBS-28}$	$\delta^{30}Si_{NBS-28}$
PR892_Met8	−7.16	−8.23	−2.90	−7.36	−8.55
PR892_Met9	−7.08	−7.82	−3.03	−7.29	−8.13
PR892_Met10	−7.26	−8.25	−2.98	−7.46	−8.57
PR892_Sil8	−5.95	−5.85	−2.92	−6.15	−6.16
PR892_Sil9	−6.23	−6.46	−2.89	−6.44	−6.77
PR892_Sil10	−6.29	−6.65	−2.85	−6.49	−6.96
PR892_Sil11	−6.00	−5.96	−2.92	−6.21	−6.27
PR892_Met6	−7.32	−8.52	−2.91	−7.52	−8.84
PR892_Met7	−7.35	−8.28	−3.06	−7.55	−8.60

[a] USNM is San Carlos olivine which is used as an in house standard used for laser ablation analyses.

experiments, it will be discussed in more detail in Section 4.2, below.

4.1.2. PR892 and PL613

These experiments are at 7 GPa and are all in a solid-melt regime. That is, the fractionation is between crystalline olivine and iron melt. Isotope ratios collected on any given analytical session for PL613 experiment show little scatter, however there is a clear distinction between the two analytical sessions. While the absolute values for each of these analysis days differ by approximately 0.7 per mil, the difference between metal and silicate (0.95‰ vs. 0.91‰ for December 2010 and January 2011, respectively) is reproduced well within error. We infer that the difference between the two analytical sessions was due to less than optimal torch position (see Section 2) or some sort of drift in the mass spectrometer. However, here again the silicate–metal fractionation is the same within analytical uncertainties for the two analytical sessions. It is the difference between the metal and silicate that matters. The fractionation factor is taken to be the average of the two sets of data. We emphasize that even at 2200 °C the fractionation in Si isotope ratios is still ~1.0‰ (~0.5 per mil per amu). If the data are divided into two separate days (Fig. 4c) the scatter associated with each day is within the error of analysis. Therefore, at 2200 °C 20 min is sufficient to attain equilibrium even when in the solid state.

4.2. Isotopic equilibrium

Time is a crucial variable in high P/T isotope equilibration experiments. While previous high-pressure experiments on silicate–metal partitioning have been run for tens of seconds to several minutes in order to minimize capsule interaction, isotope experiments require much longer durations in order to reach equilibrium, or even trend towards equilibrium (Shahar et al., 2008, 2009).

In the current study we have duplicated the results of Shahar et al. (2009) and shown that we obtain the same silicate–metal fractionation factor after 60 min that were previously obtained after 30 min. We conclude that 30 min is sufficient at 1800 °C for Si isotopic equilibration between liquid silicate and metal. As the other experiments in this study were conducted at higher temperatures, the duration of the experiments reported here should be sufficient to achieve isotopic equilibrium.

Fig. 5 shows the average $\delta^{29}Si$ and $\delta^{30}Si$ values for the three experiments at 1800, 2000, and 2200 °C. Note that the silicate values agree in all three cases. This is because the vast majority of the Si in the system resides in the silicate, meaning that the silicate is acting in effect as an infinite reservoir of Si; exchange of Si isotopes in silicate with Si in metal can have no detectable effect on the composition of this infinite reservoir. As expected, it is the isotopic composition of Si in metal that changes to achieve isotopic equilibrium between the two phases. The metal $\delta^{29}Si$ and $\delta^{30}Si$ values increase as a function of temperature, decreasing the fractionation factor between silicate and metal as temperature increases. The regular shift in fractionation with temperature is consistent with isotopic equilibrium. Fig. 6 shows the temperature dependence of the fractionation factor between silicate and metal. The data adhere to the $1/T^2$ relationship predicted for equilibrium isotope fractionation at high temperatures (e.g., Bigeleisen and Mayer, 1947; Urey, 1947).

The experimental temperature dependence is plotted alongside the theoretical curve for the olivine–FeSi fractionation as calculated by Georg et al. (2007) and the curve based on meteoritic data as determined by Ziegler et al. (2010). We note that the fractionation factor at 1800 °C was at 1 GPa while the two at 2000 and 2200 °C were at 7 GPa but the three are in excellent agreement with the theory and with each other (they are consistent with a single line of temperature dependence), implying that the 6 GPa difference did not cause a significant isotope fractionation as predicted by Shahar et al. (2009). In addition, the current results between olivine and metal are in excellent agreement with previous results between liquid silicate and metal (see above), implying that the fractionation factor between silicate melt and olivine is insignificant at these conditions. The temperature dependence of fractionation obtained by these experiments is $\Delta^{30}Si_{silicate-metal} = 7.45 \pm 0.41 \times 10^6/T^2$, in excellent agreement with both theoretical calculations for olivine–Fe-rich metal (Georg et al., 2007) and the observed fractionation between enstatite and Fe–Ni-rich metal in reduced enstatite meteorites (Ziegler et al., 2010).This agreement suggests that the Si isotope fractionation between silicate and Fe-rich metal is similar, although perhaps not identical, regardless of the precise compositions and structures of the silicate and metal phases.

In order to obtain the values for $\Delta^{30}Si_{silicate-metal}$ all of the individual $\delta^{30}Si$ values for each experiment were averaged. There are local deviations in the isotopic composition of each experiment (e.g., Fig. 7). The source of this dispersion is probably due to local deviations in bulk composition

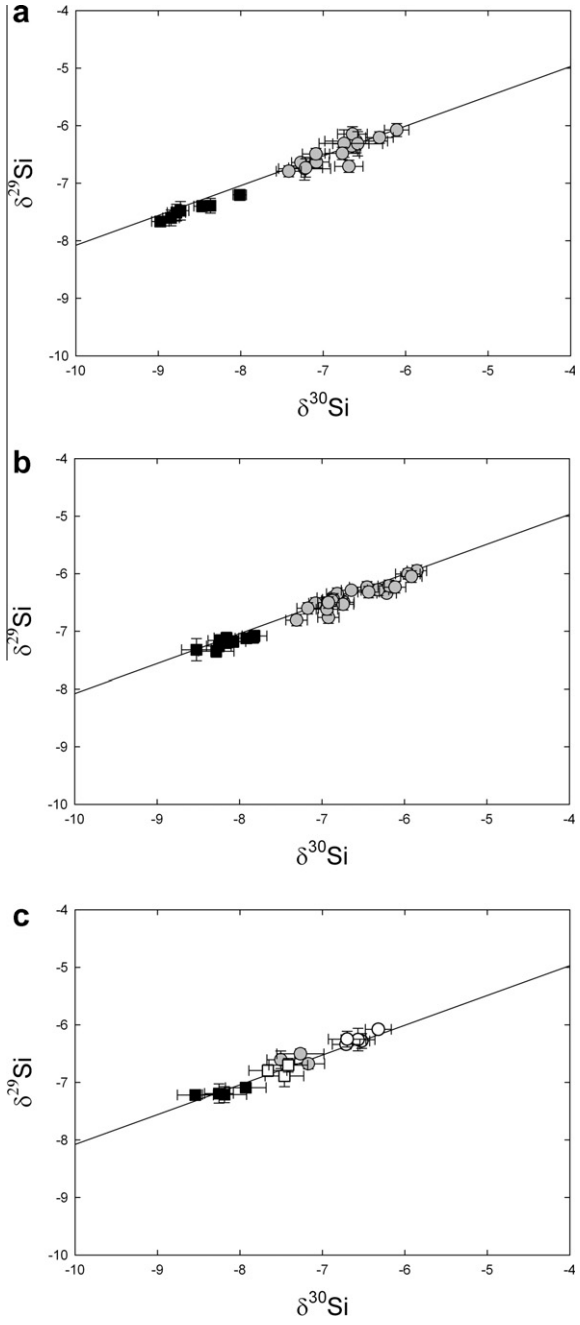

Fig. 4. Three isotope plots of experiments PC871 (a), PR892 (b), and PL613 (c). Squares represent the metal analyses and circles represent the silicate analyses. In panel c the analyses are broken into two groups indicating the two separate days of analysis (white represents one day and the gray and black the other). See the text for more detail.

due to diffusive transport of Si isotopes (into the silicate from the metal) or a kinetic effect during quenching of the experiment. Self diffusion of silicon in olivine is very slow; the characteristic length scale for self-diffusion of Si isotopes in olivine is 0.3 μm at the conditions of the experiment (Dohmen et al., 2002). As there is no pattern associated with the δ^{30}Si values we cannot at this time determine the exact reasons for this scatter however, we can deduce

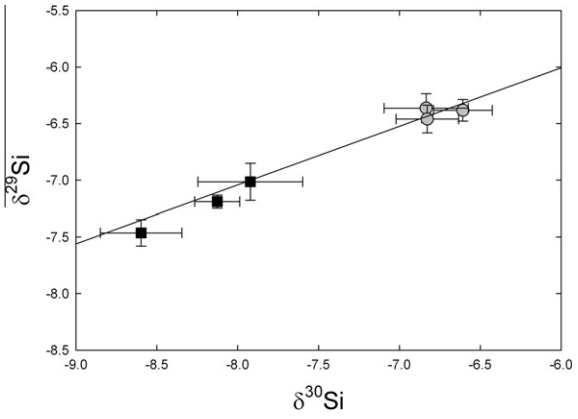

Fig. 5. A three isotope plot showing the average values of all three experiments. The silicate points overlap showing that the majority of the silicon in the experiment is in the silicates. The metal points move closer to the silicate value as the temperature increases and the fractionation decreases.

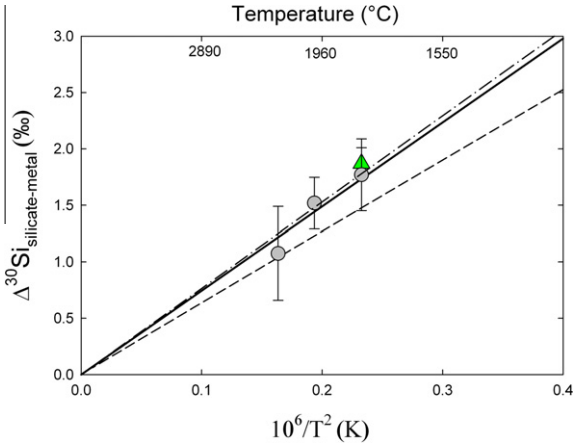

Fig. 6. The temperature dependent silicon isotope fractionation factor. The points represent the three experiments at 1800, 2000 and 2200 °C, the thick black line is the best fit line. The black dashed line is the theoretical prediction from Georg et al. (2007) and the dashed-dotted line is from Ziegler et al. (2010). The triangle is the fractionation factor from Shahar et al. (2009). All are in excellent agreement.

that it is not related to crystal, thermal gradients (such as discussed in Richter et al., 2009) or other artifacts that would effect the silicon isotopic ratios on a large scale. The variations are on the micron scale and we do not believe they affect the overall equilibrium fractionation seen between metal and silicate.

The fact that metal alloy in the experiment has δ^{29}Si and δ^{30}Si values that are on the secondary fractionation line demonstrates that there was substantial exchange between the Si in the silicate and Si in the metal. The existence of a chemical gradient in the experiment may have accelerated the diffusion of Si in the olivine by replacing self-diffusion with chemical diffusion, but quenching the experiment seems to have caused some last minute variations.

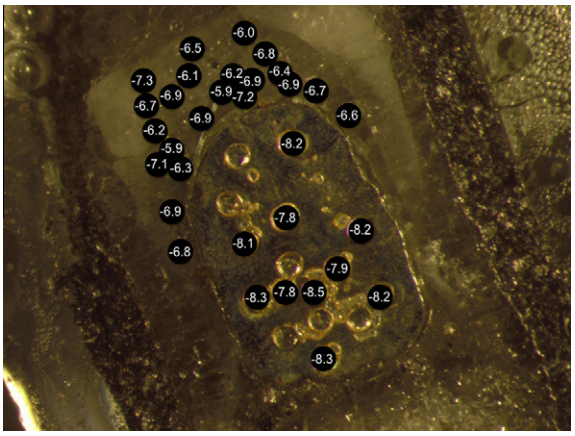

Fig. 7. A picture of PR-892 with the δ^{30}Si analyses shown in their respective positions. No trend can be seen between the values and the spatial position.

This study predicts that planets that formed under reducing conditions, such as the Earth and Mercury, would also incorporate Si into their iron cores.

4.3. Comparison to other isotopic systems

There is very limited data exploring stable isotope fractionation of the non-traditional stable isotopes experimentally at high pressure and temperature. Apart from the Si studies mentioned above, Poitrasson et al. (2009) suggest that there is no iron isotope fractionation at high pressure and temperature between metal and silicate, when theoretical studies predict there should be a small fractionation (e.g., Polyakov, 2010). More work needs to be done in the iron system to determine if there is an iron isotopic fractionation at high temperatures.

There are, however, new studies aimed at identifying differences between the bulk silicate Earth and chondrites in several isotope systems. A recent publication (Moynier et al., 2011) found a difference of up to ~0.4‰ between meteorites and BSE in δ^{53}Cr, implying that Cr was partitioned into the Earth's core and fractionated the isotopes in the process. As in the silicon system, an experimental calibration of the silicate–metal partitioning of Cr isotopes is warranted to assess the viability of a Cr isotope effect during core formation. All of this research is based on the assumption that the Earth started with a chondritic composition and that any difference seen today between Earth and chondrite is directly related to a physical or chemical process in Earth's history. By combining experiments, theoretical calculations, and analyses of natural samples we can begin to understand why isotopic systems behave differently at high pressure and temperature.

5. CONCLUSIONS

Combining high *P–T* experiments with stable isotope analyses is a useful way to understand the mechanisms responsible for non-traditional stable isotope fractionation, providing new constraints on Earth differentiation processes. In this study we present new experiments showing that there is a Si isotope fractionation between metal and silicate at high pressure and temperature. We further demonstrate that there are advantages to measuring isotope fractionation in systems closed to loss of the analyte. A comparison between these new results and our previous study shows that open-system behavior does not necessarily preclude isotopic equilibration, though it is not ideal. These new experimental results demonstrate that Si isotope fractionation between silicate and Fe-rich metal is rather insensitive to the precise composition and structure of the silicate or the metal, and that pressure effects are small if present at all between 1 and 7 GPa. We have also shown that laser ablation MC-ICPMS can be a valuable tool for measuring isotope ratios in high *P–T* experimental run products if the samples are large enough and the laser ablation technique has been verified.

Studies of simple systems such as these where the fractionation is amenable to calculations as well as experimentation represent a good way forward for honing the experimental approaches that work best. As we continue to slowly build up a database of experimentally determined fractionation factors and combine them with *ab initio* calculations we can begin to answer fundamental questions about the utility of stable isotopes as monitors of planetary differentiation.

ACKNOWLEDGEMENTS

This work was supported by NSF grant (EAR0948131) to A.S. and L.D. John Armstrong is thanked for performing the thin film calculations and for assistance on the microprobe and the SEM. This paper greatly benefited from reviews by Mathieu Roskosz, Bastian Georg, an anonymous reviewer and the editorial handling of Frederic Moynier.

REFERENCES

Armytage R. M. G., Georg R. B., Savage P. S., Williams H. M. and Halliday A. N. (2011) Silicon isotopes in meteorites and planetary core formation. *Geochim. Cosmochim. Acta.* **75**, 3662–3676.

Bertka C. M. and Fei Y. (1997) Mineralogy of Martian interior up to core–mantle boundary pressures. *J. Geophys. Res.* **102**, 5251–5264.

Bigeleisen J. and Mayer M. G. (1947) Equilibrium constants for isotopic exchange reactions. *J. Chem. Phys.* **15**, 261–267.

Chakrabarti R. and Jacobsen S. B. (2010) Silicon isotopes in the inner Solar System: implications for core formation, solar nebular processes and partial melting. *Earth Planet. Sci. Lett.* **74**, 6921–6933.

Chmeleff J., Horn I., Steinhoefel G. and von Blanckenburg F. (2008) In situ determination of precise stable Si isotope ratios by UV-femtosecond laser ablation high-resolution multi-collector ICP-MS. *Chem. Geol.* **249**, 155–166.

Dohmen R., Chakraborty S. and Becker H.-W. (2002) Si and O diffusion in olivine and implications for characterizing plastic flow in the mantle. *Geophys. Res. Lett.* **29**, 2030–2034.

Fitoussi C., Bourdon B., Kleine T., Oberli F. and Reynolds B. C. (2009) Si isotope systematics of meteorites and terrestrial peridotites: implications for Mg/Si fractionation in the solar nebula and for Si in the Earth's core. *Earth Planet. Sci. Lett.* **287**, 77–85.

Georg R. B., Halliday A. N., Schauble E. A. and Reynolds B. C. (2007) Silicon in the Earth's core. *Nature* **447**, 1102–1106.

Geßmann C. K. and Rubie D. C. (1998) The effect of temperature on the partitioning of nickel, cobalt, manganese, chromium, and vanadium at 9 GPa and constraints on formation of the Earth's core. *Geochim. Cosmochim. Acta* **62**, 867–882.

Hillgren V. J., Gessmann C. K. and Li J. (2000) An experimental perspective on the light element in Earth's core. In *Origin of the Earth and Moon* (eds. R. M. Canup and K. Righter). University of Arizona Press, Tucson, AZ, pp. 245–264.

Li J. and Fei Y. (2004) Experimental constraints on core composition. *Treatise on Geochemistry* **2**, 521–546.

Matsuhisa J., Goldsmith J. R. and Clayton R. N. (1978) Mechanisms of hydrothermal crystallisation of quartz at 250 °C and 15 kbar. *Geochim. Cosmochim. Acta* **42**, 173–182.

Moynier F., Yin Q. Z. and Schauble E. (2011) Isotopic evidence of Cr partitioning into Earth's core. *Science* **331**, 1417–1420.

O'Neill H. S. C., Canil D. and Rubie D. C. (1998) Oxide–metal equilibrium to 2500 °C and 25 GPa: implications for core formation and the light component in the Earth's core. *J. Geophys. Res.* **103**, 12,237–12,260.

Palme H. and O'Neil H. S. C. (2003) Cosmochemical estimates of mantle composition. In *Treatise on Geochmistry*, vol. 2, (eds. H. D. Holland and K. K. Turekian) Elsevier, Amsterdam (Chapter 1).

Pearson N.J., Griffin W.L. and O'Reilly S.Y. (2008) Mass fractionation correction in laser ablation multiple-collector ICP-MS: implications for overlap corrections and precise and accurate in situ isotope ratio measurement. SC Vol. 40. In *Laser Ablation ICP–MS in the Earth Sciences: Current Practices and Outstanding Issues* (ed. P. Sylvester). p. 356. ISBN 9-0-921294-49-8.

Poitrasson F., Roskosz M. and Corgne A. (2009) No iron isotope fractionation between molten alloys and silicate melt to 2000 °C and 7.7 GPa: experimental evidence and implications for planetary differentiation and accretion. *Earth Planet. Sci. Lett.* **278**, 376–385.

Polyakov V. B. (2010) Equilibrium iron isotope fractionation at core–mantle boundary conditions. *Science* **323**, 912–914.

Richter F. M., Dauphas N. and Teng F. Z. (2009) Non-traditional fractionation of non-traditional isotopes: evaporation, chemical diffusion and soret diffusion. *Chem. Geol.* **15**, 92–103.

Savage P. S., Georg R. B., Armytage R. M. G., Williams H. M. and Halliday A. N. (2010) Silicon isotope homogeneity in the mantle. *Earth Planet. Sci. Lett.* **295**, 139–146.

Shahar A. and Young E. D. (2007) Astrophysics of CAI formation as revealed by silicon isotope LA-MC-ICPMS of an igneous CAI. *Earth Planet. Sci. Lett.* **257**, 497–510.

Shahar A., Young E. D. and Manning C. E. (2008) Equilibrium high-temperature Fe isotope fractionation between fayalite and magnetite: an experimental calibration. *Earth Planet. Sci. Lett.* **268**, 330–338.

Shahar A., Ziegler K., Young E. D., Ricolleau A., Schauble E. A. and Fei Y. (2009) Experimentally determined Si isotope fractionation between silicate and Fe metal and implications for Earth's core formation. *Earth Planet. Sci. Lett.* **288**, 228–234.

Urey H. C. (1947) The thermodynamic properties of isotopic substances. *J. Chem. Soc.*, 562–581.

Wade J. and Wood B. J. (2005) Core formation and the oxidation state of the Earth. *Earth Planet. Sci. Lett.* **236**, 78–95.

Ziegler K., Young E. D., Schauble E. A. and Wasson J. T. (2010) Metal–silicate silicon isotope fractionation in enstatite meteorites and constraints on Earth's core formation. *Earth Planet. Sci. Lett.* **295**, 487–496.

Associate editor: Frederic Moynier